Full length article

Growth of BiSb on GaAs (001) and (111)A surfaces: A joint experimental and theoretical study

Dima Sadek, Antoine Jay, Jihan El Hila, Quentin Gravelier, Alexandre Arnoult, Rémi Demoulin, Filadelfo Cristiano, Sébastien Plissard, Anne Hémeryck *

LAAS-CNRS, Université de Toulouse, CNRS, Toulouse, France

ARTICLE INFO

ABSTRACT

The integration of the $Bi_{1-x}Sb_x$ topological insulator on GaAs is studied both experimentally and theoretically on (001) and (111)A surfaces. The molecular beam epitaxy of thin $Bi_{0.9}Sb_{0.1}$ layer on both substrates leads to the observation of different growth modes: Volmer Weber for GaAs(001) and Stranski–Krastanov for GaAs (111)A. By first principles calculations, we corroborate these observations. On the (001) surface at the early stages of deposition, we show that Bi atoms diffuse more easily until they agglomerate to form isolated islands on the surface, favoring a 3D growth. Here, each island can have an independent growth direction. On contrary, the diffusion of Bi atoms on the (111)A surface is limited: it is favorable for Bi atoms to bond directly with GaAs, creating thus a wetting layer before a further Stranski–Krastanov growth.

1. Introduction

Topological insulators (TIs) have attracted much attention over the last decades due to their unique physical properties [1]. What distinguishes these materials from ordinary insulators is the presence of gapless metallic states topologically protected from disorder at their edge or surface [2,3]. These states have a chiral nature similar to that of a quantum Hall system, but with unconventional spin textures [4]. This means that the spin orientation of carriers is locked perpendicular to their propagation. There are two kinds of TIs: the strong ones (non-trivial) that stand out from the weak ones (trivial) by the odd number of crossings between the Fermi level and the surface states. This prevents the metallic surface states from being gapped even in the presence of non-magnetic perturbations [5] and regardless of the chemical potential [4]. In their pioneer article, Fu and Kane predicted that $Bi_{1-x}Sb_x$ behaves as a strong TI [6]. Shortly after this theoretical proposition, $Bi_{1-x}Sb_x$ becomes the first 3D TIs experimentally confirmed by Hsieh *et al.* [7]. $Bi_{1-x}Sb_x$ presents a high electrical conductivity ($\sim 10^5$ $\Omega^{-1}m^{-1}$) [8,9] and a large spin Hall angle ($\sim 52°$) [10] making it one of the most promising TIs for spintronics applications such as low-current spin–orbit torque magnetoresistive random access memories [11].

Nevertheless, the epitaxial growth of $Bi_{1-x}Sb_x$ remains a challenging task, which has limited its integration in industrial devices. Indeed, the TI behavior comes from an insulating bulk, the crystalline symmetry and a low number of defects in the material. The absence of natural substrate for $Bi_{1-x}Sb_x$ limited its integration to polycrystalline and amorphous thin layers by chemical and physical vapor deposition techniques. Moreover, even if $Bi_{1-x}Sb_x$ thin films have already been successfully grown on a GaAs (111) B [12] and A [13] surfaces, the nanoelectronics and optoelectronics industry prefers (001) oriented substrates. Different crystal structures and large mismatches (13.7%) strongly limited this integration until recent developments [14,15].

In this paper, we study the bismuth growth modes on both GaAs (001) and (111)A oriented substrates experimentally by molecular beam epitaxy (MBE) and theoretically by *ab initio* calculations. The growth mechanisms on both surfaces present clear differences leading to structurally and electronically different properties of the deposited metallic films, which is probed using transmission electron microscopy (TEM) analysis and resistivity measurements. These observations are corroborated by the *ab initio* calculations, detailing the first stages of the growth, such as the nucleation of Bi atoms on the surface, by a thorough study of the adsorption sites and the ability of the atoms to diffuse on the surface. Methods are described in Section 2. Experimental measurements are presented in Section 3. *Ab initio* results are then shown in Section 4 before a final discussion in Section 5.

---

2. Methods

2.1. Preparation of the GaAs (001) and (111)A surfaces

One of the most important steps that contribute to define the quality and morphology of the growth layer is the substrate surface preparation. That of the GaAs (001) substrate used in our work is based on several successive steps. Once the 2 inches undoped GaAs (001) wafers (350 μm-thick) from AXT are loaded into the Riber's MBE 412 system, they are transferred into the preparation chamber to be degassed at 300 °C for 1 h. Next, they are loaded into the growth chamber, where they are heated up to 635 °C, temperature for which the GaAs is known to be fully deoxidized [16–18], under an As flux of 1.2×10^{-5} Torr. Note that the As shutter opens as soon as the temperature is above 400 °C. The substrate temperature is maintained at 635 °C for 10 min to ensure that all oxide is removed. This temperature is probed by band edge thermometry from kSA BandiT. At this point, the GaAs (001) Reflection High-Energy Electron Diffraction (RHEED) pattern appears, confirming the removal of the superficial oxide layer of the GaAs substrate [14]. Next, the temperature is ramped down to 580 °C to grow a 1 μm-thick GaAs buffer layer with a V/III ratio of 2 in 1 h.

The surface preparation of the GaAs (111)A substrate is generally more complex than that of GaAs (001) due to the very low adhesion coefficient of As atoms on the Ga-terminated surface [19]. Once the surface of the 2 inches undoped GaAs (111)A wafers is degassed at the same temperature as the GaAs (001) one, the oxide on the GaAs (111)A surface is removed by heating the substrate to 635 °C under an As flux of 2×10^{-5} Torr for a temperature above 400 °C. Then, the temperature is cooled down to the GaAs buffer layer growth temperature. At this stage, the surface preparation of GaAs (111)A requires a very high As flux since As atom can only bond to one Ga atom of the outermost layer of a GaAs (111)A substrate instead of two as in the case of GaAs (001). Besides the As flux, the substrate temperature is also an important parameter to obtain smooth GaAs layers. Da Woolf *et al.*s [20] have shown that setting the substrate temperature above 560 °C or below 500 °C leads to pyramid-shaped defects and rough surface, respectively. Based on this, a GaAs buffer layer is grown with a V/III ratio of 10 at 550 °C until an atomically smooth surface is obtained (thickness of about 0.3 μm).

In both cases, once the GaAs buffer layer is grown, the temperature is cooled down to the $Bi_{1-x}Sb_x$ growth temperature while keeping the same As flux on for temperatures above 400 °C (1.2×10^{-5} Torr for GaAs (001) and 2×10^{-5} Torr for GaAs (111)A). After temperature stabilization, $Bi_{1-x}Sb_x$ growth is initiated (terminated) by opening (closing) simultaneously the Bi and Sb shutters. According to the RHEED records, a change in temperature leads to the GaAs (001) surface reconstruction transitioning from $\beta_2(2 \times 4)$ to $c(4 \times 4)$ when the temperature is below 505 °C [21] while GaAs (111)A exhibits only the (2×2) surface reconstruction, even at low temperature, which is in agreement with [20]. In this study, the composition of the bismuth antimonide is $Bi_{0.9}Sb_{0.1}$. Further details can be found in Ref. [14,15]. A complementary analysis of the Bi/Sb ratio by energy dispersion spectroscopy (EDS) performed in a TEM is provided in Appendix A Fig. 8. The $Bi_{0.9}Sb_{0.1}$ alloy composition is chosen constant for the whole study.

2.2. GaAs surfaces modeling

The GaAs (001) and (111)A surfaces have been modeled using respectively a 172-atom orthorhombic supercell and a 188-atom hexagonal supercell of diamond-like GaAs repeated periodically in the three dimensions. The surface reconstructions have been chosen to be As-rich, as suggested by the experimental V/III ratio. A 20 Å thick vacuum space has been added on top of the bulks to create the slabs and respectively 32 and 16 hydrogen atoms have been added under the bottom layer to passivate each dangling bond. The two supercells are finally defined as $Ga_{64}As_{76}H_{32}$ (001) and $Ga_{80}As_{92}H_{16}$ (111)A.

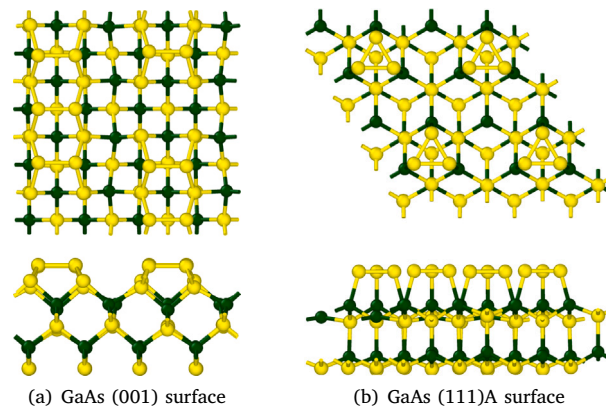(a) GaAs (001) surface   (b) GaAs (111)A surface

Fig. 1. Top and side views of the supercells used for the modeling of (a) the GaAs (001) surface and (b) the GaAs (111)A surface. For clarity, only the topmost layers are represented. Yellow and green spheres represent As and Ga atoms, respectively.

The atomic positions of the two bottom GaAs layers are fixed at their calculated positions in the diamond-like bulk (Ga–As distance=2.39 Å), while all the other atomic positions are allowed to relax freely. As atoms have been added above the surface to obtain the As-rich surface reconstructions. The reconstruction of the As-rich (001) surface leads to the $c(4 \times 4)\beta$ structure [22–26], composed of two [1$\bar{1}$0] rows of As–As dimers separated by a so-called channel. One As–As dimer is missing every three dimers (Fig. 1(a)). The reconstruction of the (111)A As-rich surface leads to the $\beta(2 \times 2)$ with the As–As–As trimer structure [27,28] featured by four trimers above the Ga–As top layer (Fig. 1(b)).

2.3. Computational details

Total energy calculations have been performed within the density functional theory (DFT) [29,30], in the pseudopotential and plane waves approach as implemented in Quantum Espresso 7.0 [31] with the general gradient approximation (GGA [32]) for the exchange and correlation functional. The core electrons are represented by the projector-augmented wave (PAW) potentials [33]. The energy cutoff is set at 70 eV and the Brillouin Zone has been sampled at zone center only (Γ point) inducing an accuracy of 2 meV/at.

The theoretical study conducted is only detailed for Bi. It should be noted that a similar study has been conducted with Sb (with the same calculation parameters. Results on Sb adsorption energies are provided in Appendix B Figs. 9 and 10), the trends observed are the same and do not change the main conclusions of this work. We also consider that Bi concentration *vs.* Sb concentration dominates in the early stages of deposition and that the coupled effects of Bi/Sb at higher coverage is out of the scope of this paper.

The thermodynamically stable sites for the Bi adsorbed atoms have been found by adding a Bi atom 4 Å above the surface on different positions sampled over the symmetrically reduced supercell. All the unfixed atomic positions are then relaxed while fixing the supercell parameters. The addition of the *n-th* Bi atom has been done following the same sampling procedure above the reference configuration at step $n-1$. To study the island formation, the reference $n-1$ configuration is the most stable one among the ones forming an island. The adsorption is said to form an island, or agglomeration, when the added atom is bonded to a previously deposited Bi or to a dimer/trimer already bonded to a Bi atom.

The adsorption energy of n adsorbed Bi atoms has been calculated as $E_{ad}^{n} = E_{surf+nBi} - E_{surf} - nE_{Bi}$ where $E_{surf+nBi}$ is the relaxed surface with n adsorbed Bi atoms, E_{surf} the energy of the reconstructed surface without any Bi atom, and E_{Bi} the energy of one single isolated Bi atom. The same equation was used to determine the Sb adsorption
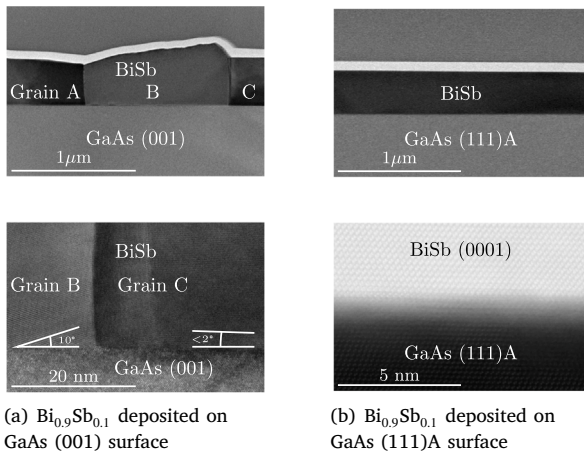
(a) Bi$_{0.9}$Sb$_{0.1}$ deposited on GaAs (001) surface

(b) Bi$_{0.9}$Sb$_{0.1}$ deposited on GaAs (111)A surface

Fig. 2. Transversal TEM images of the Bi$_{0.9}$Sb$_{0.1}$ deposition on top of (a) the GaAs (001) surface and (b) GaAs (111)A surface.

Fig. 3. Variation of the sample resistivity for different Bi$_{0.9}$Sb$_{0.1}$ thicknesses on the GaAs (001) (black) and GaAs (111)A (red) surfaces.

energies provided in Appendix B Figs. 9 and 10. The relative adsorption energy of the *n-th* atom is defined as $E_{ad,rel}^n = E_{surf+nBi} - E_{surf+(n-1)Bi}$ where $(n-1)$ is the most stable structure containing $(n-1)$ adsorbed Bi atoms. In the following, we also use ΔE to compare the stability of two atomic configurations at a given Bi coverage. The activation–relaxation technique as coupled with DFT approach (ARTn [34,35]) has been used to calculate the energy barriers E_b of the Bi diffusion between the stable surface positions.

3. Experimental results: different BiSb growth modes depending on the orientation of the GaAs substrate

The addition of Bi and Sb atoms on the GaAs (001) surface leads to the formation of many Bi$_{0.9}$Sb$_{0.1}$ grains on the surface (Fig. 2(a) top panel). These grains have different growth orientations (Fig. 2(a) bottom panel) such that the Bi$_{0.9}$Sb$_{0.1}$ (0001) growth direction is not parallel to the GaAs (001) one. The angle between the GaAs (001) surface and the Bi$_{0.9}$Sb$_{0.1}$ (0001) one has a huge variability ranging from 0 to 40°. This implies that the grains merge together forming twins at the grain boundaries. On the contrary, the addition of Bi and Sb atoms on the GaAs (111)A surface leads to the formation of a thin clean Bi$_{0.9}$Sb$_{0.1}$ film (Fig. 2(b) top panel) for which the Bi$_{0.9}$Sb$_{0.1}$ (0001) growth direction is parallel to the GaAs (111) one (Fig. 2(b) bottom panel).

The resistivity of the samples has been measured for different thicknesses as described in Ref. [15]. Before the Bi$_{0.9}$Sb$_{0.1}$ epitaxy, the resistivity of the sample is the one of the semiconducting bulk GaAs. It then decreases drastically when the Bi$_{0.9}$Sb$_{0.1}$ totally covers the surface allowing thus the electrons to freely travel into the layer. The overall evolution of this resistivity as a function of the deposited Bi$_{0.9}$Sb$_{0.1}$ thickness (Fig. 3) is not the same for the two surfaces. On the (111)A surface, the decrease of resistivity quickly appears, after the deposition of 5–10 nm of Bi$_{0.9}$Sb$_{0.1}$, which suggests a uniform distribution of the deposited atoms as atomic scale layers. On the (001) surface, this decrease appears later, after the deposition of 20–30 nm. This suggests a non uniform growth mode where the deposited atoms do not form early a connected layer, but agglomerate into isolated islands before coalescence, as confirmed in our previous work [15]. We note that topological surface states of BiSb are known to appear above 2.5 nm [36], but the resistivity of the wetting layer in Fig. 3 decreases only above 5 nm due to the roughness of the sample surface that prevents the BiSb surface conduction channels for centimeter large devices. *In situ* strain measurements during growth [37] validate this conclusion of two distinct growth modes. The curves are presented in Appendix C,
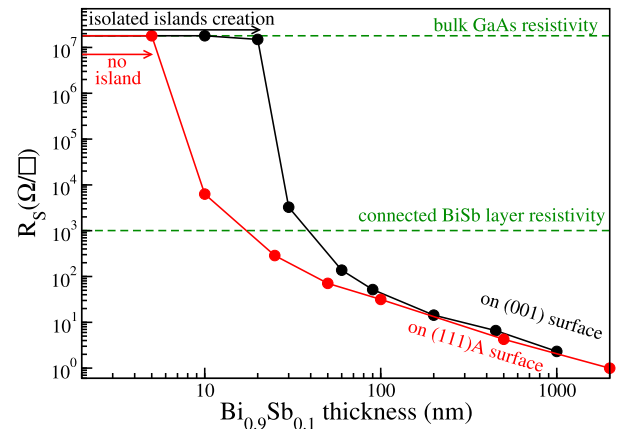
where the changes in slope of the wafer curvature observed around 20 nm on GaAs (001) and around 4 nm on GaAs (111)A correspond to the observations in Fig. 3.

4. DFT results

4.1. Diffusion of single adsorbed Bi atom on the surface

All stable adsorbed configurations discussed below are shown in Appendix B.

GaAs (001) surface - Four main stable adsorption sites have been identified on the GaAs (001) surface. *(i)* In the ground state site (GS^{001} Fig. 9(a), $E_{ad}^1 = -2.89$ eV), the Bi atom is located in the middle of the missing dimer, bonded to the four As atoms of the sublayer. *(ii)* In the adsorption site corresponding to the side of the missing dimer (*mds* Fig. 9(b), $\Delta E = 0.02$ eV), the Bi atom is linked to two As atoms in the sublayer and to the As atom of a dimer in the adjacent As dimers row. *(iii)* In the channel site (*ch* Fig. 9(c), $\Delta E = 1.02$ eV), the Bi atom is in the middle of the channel, bonded to one As atom on the two dimers separated by the channel and to one As atom of the sublayer. The two As–As dimers are partially broken, which explain the higher energy of this position. *(iv)* In the top dimer site (*td* Fig. 9(d), $\Delta E = 0.04$ eV) the Bi atom is above the square formed by two adjacent dimers, bonded to the four corresponding As atoms. Note that the *td* configuration can be only reached by a relaxation from a particular symmetric position above the surface, giving it a low probability to exist. All these sites have relatively similar adsorption energies that differ from each other by less than 1.02 eV.

To diffuse from one GS^{001} to a topologically equivalent GS^{001} one, a symmetric minimum energy path is obtained (Fig. 4(a)). First, the Bi atom escapes from the GS^{001} configuration to reach a *mds* site. Then from the *mds* site the Bi atom passes through a *ch* configuration in the channel. From this configuration, the Bi atom continues to diffuse by a diffusion path symmetric to the first part, passing successively from a *ch* site in the vicinity of the first one encountered in the same channel, a new missing dimer *mds* and finally to the middle of the new missing dimer on a GS^{001} site. The maximum energy barrier along this path is $E_b = 1.10$ eV above the ground state. At the temperatures considered in the growth technological process (around 700 K), this energy barrier allows the easy diffusion of Bi atoms on the whole GaAs (001) surface. The *td* site is not necessary for the diffusion as it requires much higher energies ($E_b^{GS^{001} \rightarrow td} = 1.29$ eV, $E_b^{td \rightarrow td} = 1.24$ eV, $E_b^{ch \rightarrow td} = 1.00$ eV).

The diffusion of Bi atoms on the GaAs (001) surface is in contrast to its diffusion on the Si (001) surface that occurs only in one dimension along the channels [38], because the Bi atoms cannot cross the dimer rows. On GaAs (001), the Bi atom takes advantage of the surface
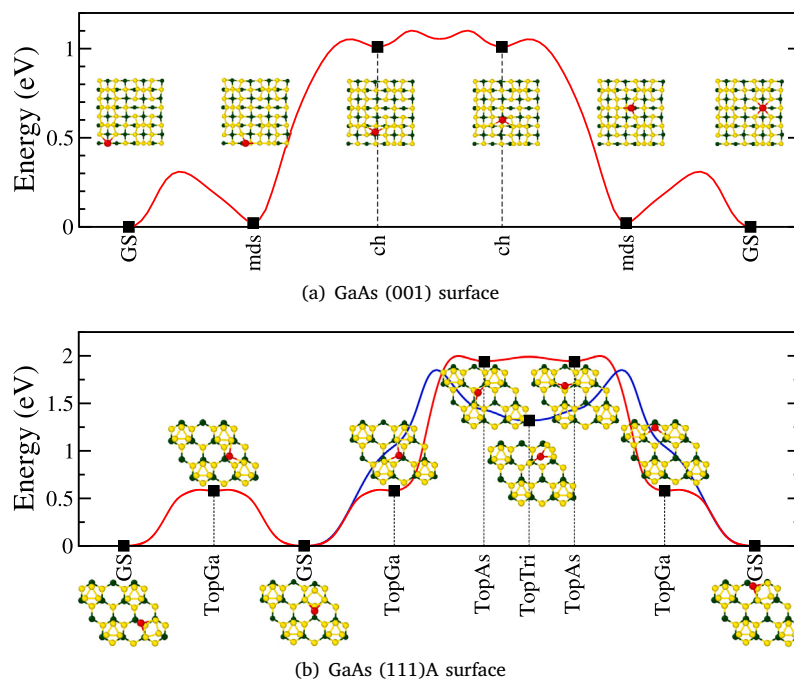
(a) GaAs (001) surface

(b) GaAs (111)A surface

Fig. 4. Minimum energy pathways of the Bi atom between the ground state positions above the (a) GaAs (001) and (b) GaAs (111)A surfaces. Red ball represent the adsorbed Bi atom.
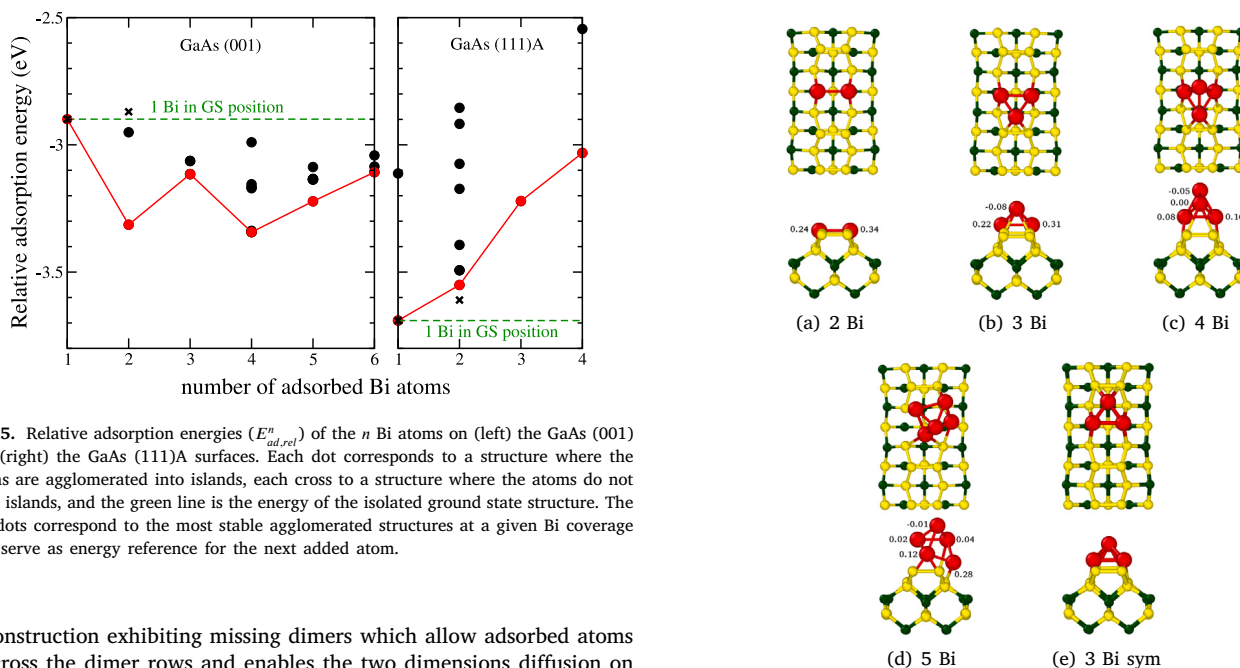

Fig. 5. Relative adsorption energies ($E_{ad,rel}^n$) of the n Bi atoms on (left) the GaAs (001) and (right) the GaAs (111)A surfaces. Each dot corresponds to a structure where the atoms are agglomerated into islands, each cross to a structure where the atoms do not form islands, and the green line is the energy of the isolated ground state structure. The red dots correspond to the most stable agglomerated structures at a given Bi coverage that serve as energy reference for the next added atom.

reconstruction exhibiting missing dimers which allow adsorbed atoms to cross the dimer rows and enables the two dimensions diffusion on the surface.

GaAs (111)A surface - Four stable adsorption sites have been found on the GaAs (111)A surface: *(i)* In the ground state site (GS^{111} Fig. 10(a), $E_{ad}^1 = -3.69$ eV), under the effect of adsorption, the Bi atom has broken one of the bonds of the trimer and is bonded to two As atoms of this trimer and to a Ga of the sublayer. *(ii)* and *(iii)* In the top Ga adsorbed site ($TopGa$ Fig. 10(b), ΔE=0.57 eV) and top As adsorbed site ($TopAs$ Fig. 10(c), ΔE=1.94 eV), the Bi atom is bonded to one Ga atom (resp. to one As atom with non-covalent bond) of the sublayer and bonded to two different trimers. *(iv)* In the so-called top trimer adsorbed site ($TopTri$ Fig. 10(d), ΔE=1.29 eV), the Bi atom is on top of the trimer, changing its geometry from equilateral to isosceles-like

(a) 2 Bi (b) 3 Bi (c) 4 Bi

(d) 5 Bi (e) 3 Bi sym

Fig. 6. Most stable atomic configurations of the agglomeration of two to five Bi atoms on the GaAs (001). Structures 3 and 5 can exist symmetrically, and an example is given for structure 3 panel 6(e). Variation of Bader charge is given on each adsorbed Bi atom in reference to the value of Bi in its pseudopotential.

breaking two As–As bonds of the trimer. Each site can be reproduced three times per trimer due to their centro-symmetry.

To diffuse from one GS^{111} to another topologically equivalent one on the GaAs(111)A surface, two minimum energy paths have been found with a similar energy barrier. In the first one, the Bi atom
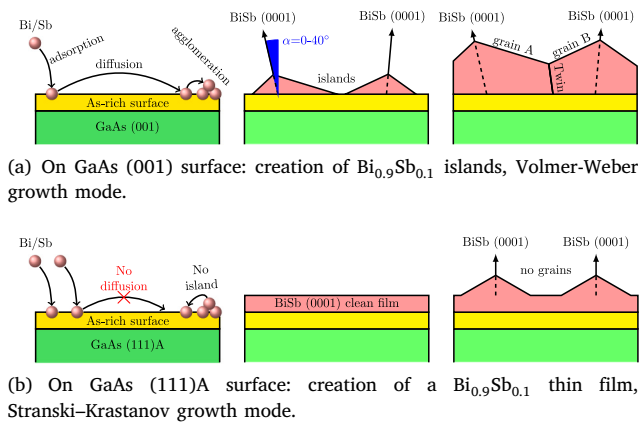
(a) On GaAs (001) surface: creation of $Bi_{0.9}Sb_{0.1}$ islands, Volmer-Weber growth mode.

(b) On GaAs (111)A surface: creation of a $Bi_{0.9}Sb_{0.1}$ thin film, Stranski–Krastanov growth mode.

Fig. 7. Schema of the two different growth modes.

diffuses by contouring the trimers passing through the intermediate configurations according to the sequence $TopGa, TopAs, TopAs, TopGa$ (Fig. 4(b), red curve, $E_b = 1.99$ eV), while in the second one, it diffuses by passing over the As-trimer using the adsorbed configuration $TopTri$ (Fig. 4(b), blue curve, $E_b = 1.84$ eV). In both cases, the energy barrier is high to move a Bi atom from a GS^{111} configuration. Under the conditions of the growth process, this energy barrier is too high to be overcome and prevents the diffusion of Bi on the surface once it has reached the GS^{111} configuration.

The Bi atom is, as As, an element of column V. Its bonding with Ga is then favored (III/V) than with As (V/V) to fill the electron deficiency. This can be seen by the lowest adsorption energy on the GS^{111} site, where a Bi–Ga bond is formed, than on the GS^{001} site, where only Bi–As are formed. This stronger bonding is harder to break and then requires a higher energy barrier to be broken, which explains the drastic difference in the diffusion capacity over the two surfaces.

4.2. 3D islands versus isolated atoms

To verify the tendency to form 3D Bi islands or a 2D Bi deposited layer, the thermodynamic stability of the Bi agglomeration is investigated by increasing the Bi coverage on both surfaces. Up to six Bi atoms were added on different positions of the two surfaces, both on isolated positions on the surface, and on configurations where one or more atoms are already adsorbed or agglomerated.

The energies of the structures that have relaxed into an island are represented by dots in Fig. 5. In this figure, if the relative adsorption energy is lower than that of the isolated atom (green dashed curve), the agglomeration into an island is favored, otherwise, the agglomeration is thermodynamically metastable which implies that islands do not form.

On the GaAs (111)A surface, none of the tested island structures are thermodynamically stable. Prior to coalescence, it is always more favorable to have isolated adsorbed atoms in the GS^{111} sites than an agglomeration (see cross on Fig. 5-GaAs (111)A). The expected growth mode tends to fill these empty sites to form a 2D layer on the surface.

On the GaAs (001) surface, several of the tested island structures are thermodynamically stable, more favorable than positioning single atoms (see cross on Fig. 5-GaAs (001)). Already, starting from the third adsorbed Bi atom, the structure starts to be 3D (see next section). The expected growth mode is then island formation.

4.3. Growth orientation on GaAs(001)

Bader charge and electron density analysis show that the Bi–Bi dimer formed when n=2 Bi is strongly bonded to the surface by covalent bonds (Fig. 6(a): 0.24 and 0.34 exchanged electrons). However,

the addition of Bi atoms drastically reduces this binding energy from n=3 (Fig. 6(b)) to n=4 (Fig. 6(c)). Indeed, these Bi atoms create a metallic island of crystalline Bi, where Bi atoms have all their electrons. The Bader charge analysis shows that the electron sharing between the surface and the bottom of the Bi island is reduced compared to the n=2 Bi case, thus reducing the binding energy with the surface. We note that after the formation of the Bi–Bi dimer in the position of the missing dimer (Fig. 6(a)), the third Bi atom favorable for clustering can be placed equiprobably on its both symmetric sides (Figs. 6(b) and 6(e)) and results in different orientations of the grown Bi nucleus. Each new Bi atom addition is then located either on top of the island (Fig. 6(c)) or next to it, changing its orientation again (Fig. 6(d)). The weak binding during the early stages of island formation implies that the island has the possibility to reorient itself, as shown by the modification of its crystalline axis between n=4 and n=5 (Fig. 6(d)). Here we confirm the many different grain orientations observed in the TEM images (Fig. 2(a)).

5. Discussions

From this theoretical study, we can describe the early stages of deposition on the GaAs surface and how these early stages are decisive for the growth of BiSb islands and then layers.

On the GaAs (001) surface, the high diffusion rate of the Bi atoms allows their agglomeration into thermodynamically stable islands (Fig. 7(a) panel 1). These observations corroborate with a Volmer-Weber growth mode. Several orientations during the nucleation of the 3D islands can appear (Fig. 7(a) panel 2), which implies a large variability of the measured angle (from 0 to 40°) with respect to the surface as observed experimentally [14]. When two neighboring islands with different growth orientations collapse, they form twins at the grain boundaries (Fig. 7(a), last panel) as shown by TEM images.

On the contrary, on the GaAs (111)A surface, the kinetic calculations show that the Bi atoms do not diffuse and the thermodynamic calculations show that their agglomeration is metastable (Fig. 7(b) panel 1), which implies that Bi islands are not formed during the initial stages of deposition, and that a wetting 2D layer of Bi atoms tends to be formed in contact with the GaAs (111)A substrate (Fig. 7(b) panel 2). It has been observed by scanning electron microscopy (not shown), that once the BiSb film has been fully connected, the surface chemical potential leads to the formation of facets (Fig. 7(b) panel 3). These observations corroborate with a Stranski–Krastanov growth mode along the <0001> direction.

6. Conclusion

In this study, we explain with the help of DFT calculations, the first steps of the growth of BiSb thin films on GaAs (001) and (111)A surfaces which then control the quality of the thin films deposited by MBE. In particular, it is shown that the way atoms deposit and diffuse on the two surfaces affects the agglomeration of the deposited atoms, favoring or not the formation of islands. The characteristic reconstruction of the GaAs (001) surfaces leads to the growth of BiSb islands, presenting a high degree of freedom for their orientation, and thus leading to the deposition of misoriented grains following a Volmer-Weber growth mode. In the case of the GaAs (111)A surface, the mixed atomic layer composed of GaAs atoms under the As-trimers surface reconstruction tends to favor the interactions of BiSb with the III element of the substrate, which prevents surface diffusion to occur. Given the two studied surfaces, we confirm the quality of BiSb films deposited on GaAs (111)A surface, conditioned by the *in situ* epitaxial conditions and then validate their strong potential for new industrial applications. Our results open new possibilities for the integration of TI at nanoscale on semiconductor substrates.

Funding sources

Declaration of competing interest

One or more of the authors of this paper have disclosed potential or pertinent conflicts of interest, which may include receipt of payment, either direct or indirect, institutional support, or association with an entity in the biomedical field which may be perceived to have potential conflict of interest with this work. For full disclosure statements refer to https://doi.org/10.1016/j.apsusc.2023.156688. Plissard reports financial support was provided by Agence Natonale de la Recherche (ANR).

Data availability

Data will be made available on request.

Acknowledgments

Appendix A. Analysis of the BiSb composition

EDS measurement have been performed from the GaAs substrate and through the BiSb grains (Fig. 8). The calculated intensities for each atom permits to know the BiSb stoichiometry: $Bi_{0.9}Sb_{0.1}$.
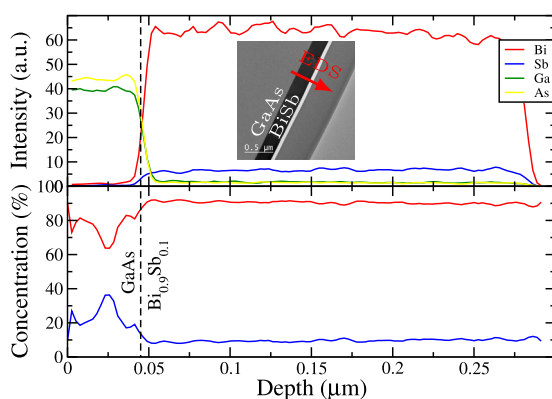

Fig. 8. Variation of the energy dispersion spectroscopy (EDS) intensities for each atom type (top panel) while crossing the BiSb grain. The beam path is represented by the red arrow on the insert transmission electron microscopy (TEM) panel. The calculated Bi and Sb concentrations (bottom panel) are calculated from there respective intensities.

Appendix B. Stable sites on the GaAs surfaces

Here are the atomic structures of the most stable sites found for the adsorption of Bi/Sb atoms on the GaAs 001) and (111)A surfaces. The values of the adsorption energies have been added for both Bi and Sb: the order of the stable structures and relative energies is the same, only the adsorption energies are shifted by ~0.15 eV for all corresponding structures.
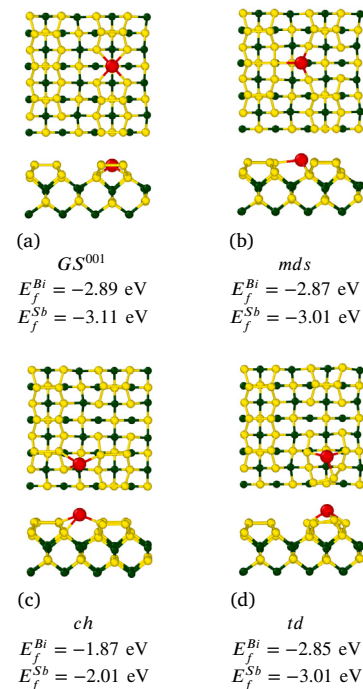

(a) GS^{001}
$E_f^{Bi} = -2.89$ eV
$E_f^{Sb} = -3.11$ eV

(b) mds
$E_f^{Bi} = -2.87$ eV
$E_f^{Sb} = -3.01$ eV

(c) ch
$E_f^{Bi} = -1.87$ eV
$E_f^{Sb} = -2.01$ eV

(d) td
$E_f^{Bi} = -2.85$ eV
$E_f^{Sb} = -3.01$ eV

Fig. 9. Stable adsorption sites on the GaAs (001) surface. Yellow, green and red spheres represent As, Ga and Bi/Sb atoms, respectively.

(a) GS^{111}
$E_f^{Bi} = -3.69$ eV
$E_f^{Sb} = -3.94$ eV

(b) $TopGa$
$E_f^{Bi} = -3.12$ eV
$E_f^{Sb} = -3.31$ eV

(c) $TopAs$
$E_f^{Bi} = -1.75$ eV
$E_f^{Sb} = -1.90$ eV

(d) $TopTri$
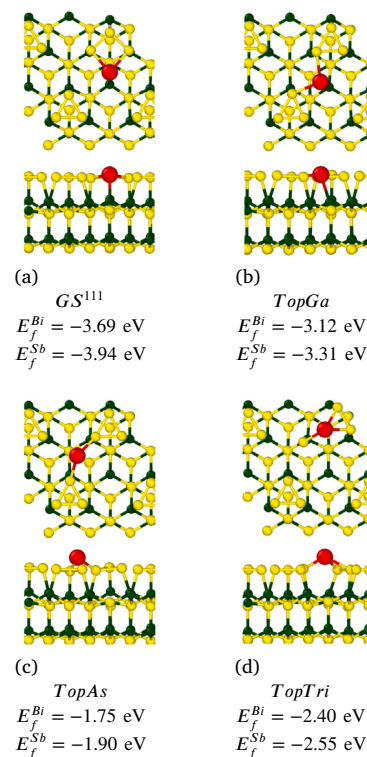$E_f^{Bi} = -2.40$ eV
$E_f^{Sb} = -2.55$ eV

Fig. 10. Stable adsorption sites on the GaAs (111)A surface. Yellow, green and red spheres represent As, Ga and Bi/Sb atoms, respectively.

Appendix C. Experimental *in situ* strain measurements during growth on GaAs (001) and GaAs (111)A

The two growth modes are further confirmed by *in situ* strain measurements [37] during growth on the two GaAs surfaces, that present totally different behaviors on both substrates (see Fig. 11).
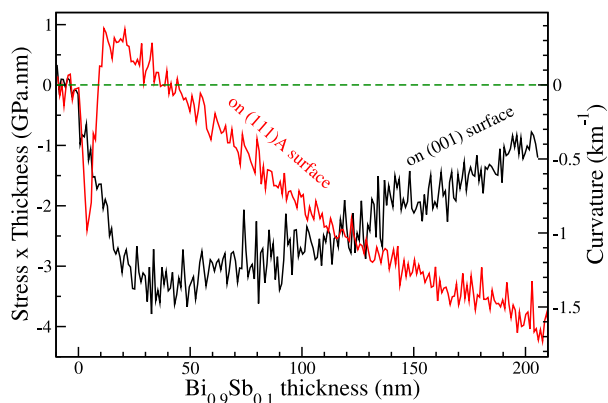
Fig. 11. Stress×thickness product (left axis), or wafer curvature (right axis), as a function of the deposited $Bi_{0.9}Sb_{0.1}$ thickness on GaAs (001) (black line) or on GaAs (111)A (red line), at 215 °C (Bi flux of 4×10^{-7} Torr and Sb flux of 5×10^{-8} Torr for both growths).

A slope change in the curvature of the wafer is observed around 20 nm on GaAs (001) and around 4 nm on GaAs (111)A, which roughly corresponds to the transitions observed electrically. This is characteristic of a drastic change of the growth mode for both surface. A compressive strain is observed during nucleation of the BiSb layer on GaAs. It can be noticed that the stress accumulates faster on GaAs (111)A than on GaAs (001). This is compatible with the presence of a BiSb wetting layer on GaAs (111)A and a Volmer Weber growth mode on GaAs (001). In both cases, the strain shifts from compressive to tensile when coalescence of nuclei occurs. It remains unclear for the moment while the strain decreases again on the GaAs (111)A oriented wafer after 20 nm.

References

[1] H.-J. Zhang, C.-X. Liu, X.-L. Qi, X.-Y. Deng, X. Dai, S.-C. Zhang, Z. Fang, Electronic structures and surface states of the topological insulator Bi 1- x Sb x, Phys. Rev. B 80 (8) (2009) 085307.

[2] J.E. Moore, The birth of topological insulators, Nature 464 (7286) (2010) 194–198.

[3] S. Tang, M.S. Dresselhaus, Electronic properties of nano-structured bismuth-antimony materials, J. Mat. Chem. C 2 (24) (2014) 4710–4726.

[4] P. Roushan, J. Seo, C.V. Parker, Y.S. Hor, D. Hsieh, D. Qian, A. Richardella, M.Z. Hasan, R.J. Cava, A. Yazdani, Topological surface states protected from backscattering by chiral spin texture, Nature 460 (7259) (2009) 1106–1109.

[5] L. Fu, C.L. Kane, E.J. Mele, Topological insulators in three dimensions, Phys. Rev. Let. 98 (10) (2007) 106803.

[6] L. Fu, C.L. Kane, Topological insulators with inversion symmetry, Phys. Rev. B 76 (4) (2007) 045302.

[7] D. Hsieh, D. Qian, L. Wray, Y. Xia, Y.S. Hor, R.J. Cava, M.Z. Hasan, A topological Dirac insulator in a quantum spin Hall phase, Nature 452 (7190) (2008) 970–974.

[8] G. Kozhemyakin, S. Zayakin, Magnetoresistance in doped Bi0. 85sb0. 15 single crystals, J. App. Phys. 122 (20) (2017) 205102.

[9] D.-X. Qu, S.K. Roberts, G.F. Chapline, Observation of huge surface hole mobility in the topological insulator Bi 0.91 Sb 0.09 (111), Phys. Rev. Let. 111 (17) (2013) 176801.

[10] N.H.D. Khang, Y. Ueda, P.N. Hai, A conductive topological insulator with large spin Hall effect for ultralow power spin–orbit torque switching, Nature Mater. 17 (9) (2018) 808–813.

[11] N.H.D. Khang, S. Nakano, T. Shirokura, Y. Miyamoto, P.N. Hai, Ultralow power spin–orbit torque magnetization switching induced by a non-epitaxial topological insulator on si substrates, Sc. Rep. 10 (1) (2020) 1–12.

[12] A. Prados, R. Ranchal, Electrodeposition of Bi thin films on n–GaAs(111)B. II. Correlation between the nucleation process and the structural and electrical properties, J. Phys. Chem. C 122 (2018) 8886–8893.

[13] K. Yao, N.H.D. Khang, P.N. Hai, Influence of crystal orientation and surface termination on the growth of BiSb thin films on GaAs substrates, J. Cr. Growth 511 (2019) 99–105.

[14] D. Sadek, D.S. Dhungana, R. Coratger, C. Durand, A. Proietti, Q. Gravelier, B. Reig, E. Daran, P.F. Fazzini, F. Cristiano, A. Arnoult, S.R. Plissard, Integration of the rhombohedral BiSb(0001) topological insulator on a cubic GaAs(001) substrate, ACS Appl. Mater. Interf. 13 (30) (2021) 36492–36498.

[15] D. Sadek, R. Daubriac, C. Durand, R. Monflier, Q. Gravelier, A. Proietti, F. Cristiano, A. Arnoult, S.R. Plissard, Structural and electrical characterizations of BiSb topological insulator layers epitaxially integrated on GaAs, Cryst. Growth Design 22 (8) (2022) 5081–5091.

[16] A.J. SpringThorpe, S.J. Ingrey, B. Emmerstorfer, P. Mandeville, W.T. Moore, Measurement of GaAs surface oxide desorption temperatures, Appl. Phys. Lett. 50 (2) (1987) 77–79.

[17] G.W. Smith, A.J. Pidduck, C.R. Whitehouse, J.L. Glasper, A.M. Keir, C. Pickering, Surface topography changes during the growth of GaAs by molecular beam epitaxy, Appl. Phys. Lett. 59 (25) (1991) 3282–3284.

[18] T. Van Buuren, M.K. Weilmeier, I. Athwal, K.M. Colbow, J.A. Mackenzie, T. Tiedje, P.C. Wong, K.A.R. Mitchell, Oxide thickness effect and surface roughening in the desorption of the oxide from GaAs, Appl. Phys. Lett. 59 (4) (1991) 464–466.

[19] S. Blanc, Matériaux III-V épitaxies sur substrats GaAs (111) pour structures laser émettant au-delà du micromètre (Ph.D. thesis), Toulouse 3, 2002.

[20] D. Woolf, D. Westwood, R. Williams, The homoepitaxial growth of GaAs (111) A and (111) B by molecular beam epitaxy: an investigation of the temperature-dependent surface reconstructions and bulk electrical conductivity transitions, Semicond. Sci. Technol. 8 (6) (1993) 1075.

[21] V.P. LaBella, M.R. Krause, Z. Ding, P.M. Thibado, Arsenic-rich GaAs (0 0 1) surface structure, Surf. Sci. Rep. 60 (1–4) (2005) 1–53.

[22] J. Neave, B. Joyce, Structure and stoichiometry of {100} GaAs surfaces during molecular beam epitaxy, J. Cr. Growth 44 (4) (1978) 387–397.

[23] R. Bachrach, R. Bauer, P. Chiaradia, G. Hansson, Surface phases of GaAs (100) and AlAs (100), J. Vac. Sc. Tech. 18 (3) (1981) 797–801.

[24] D. Chadi, C. Tanner, J. Ihm, Theoretical study of the atomic and electronic structure of the c-4×4 reconstructed GaAs (100) surface, Surf. Sci. Lett. 120 (1) (1982) L425–L430.

[25] A. Ohtake, J. Nakamura, S. Tsukamoto, N. Koguchi, A. Natori, New structure model for the GaAs(001)−$c(4 \times 4)$ surface, Phys. Rev. Let. 89 (2002) 206102.

[26] A. Ohtake, Surface reconstructions on GaAs(001), Surf. Sci. Rep. 63 (2008) 295–327.

[27] N. Moll, A. Kley, E. Pehlke, M. Scheffler, GaAs equilibrium crystal shape from first principles, Phys. Rev. B 54 (1996) 8844–8855.

[28] A. Ohtake, J. Nakamura, S. Tsukamoto, N. Koguchi, A. Natori, Surface structures of GaAs 111 A,B-(2x2), Phys. Rev. B 64 (2001) 045318.

[29] P. Hohenberg, W. Kohn, Inhomogeneous electron gas, Phys. Rev. 136 (1964) B864.

[30] W. Kohn, S.L. J., Self-consistent equations including exchange and correlation effects, Phys. Rev. 140 (1965) A1133.

[31] P. Giannozzi, O. Andreussi, T. Brumme, O. Bunau, M.B. Nardelli, M. Calandra, R. Car, C. Cavazzoni, D. Ceresoli, M. Cococcioni, N. Colonna, I. Carnimeo, A.D. Corso, S. de Gironcoli, P. Delugas, R.A. DiStasio, A. Ferretti, A. Floris, G. Fratesi, G. Fugallo, R. Gebauer, U. Gerstmann, F. Giustino, T. Gorni, J. Jia, M. Kawamura, H.-Y. Ko, A. Kokalj, E. Küçükbenli, M. Lazzeri, M. Marsili, N. Marzari, F. Mauri, N.L. Nguyen, H.-V. Nguyen, A.O. de-la Roza, L. Paulatto, S. Poncé, D. Rocca, R. Sabatini, B. Santra, M. Schlipf, A.P. Seitsonen, A. Smogunov, I. Timrov, T. Thonhauser, P. Umari, N. Vast, X. Wu, S. Baroni, Advanced capabilities for materials modelling with Quantum ESPRESSO, J. Phys.: Condens. Matter 29 (46) (2017) 465901.

[32] J. Perdew, K. Burke, M. Ernzerhof, Generalized gradient approximation made simple, Phys. Rev. Lett. 77 (1996) 3865.

[33] P.E. Blöchl, Projector augmented-wave method, Phys. Rev. B 50 (24) (1994) 17953.

[34] A. Jay, C. Huet, N. Salles, M. Gunde, L. Martin-Samos, N. Richard, G. Landa, V. Goiffon, S. de Gironcoli, A. Hémeryck, N. Mousseau, Finding reaction pathways and transition states: r-ARTn and d-ARTn as an efficient and versatile alternative to string approaches, J. Chem. Theory Comput. 16 (2020) 6726–6734.

[35] A. Jay, M. Gunde, N. Salles, M. Poberžnik, L. Martin-Samos, N. Richard, S. de Gironcoli, N. Mousseau, A. Hémeryck, Activation-Relaxation Technique: An efficient way to find minima and saddle points of potential energy surfaces, Comp. Mat. Sci. 209 (2022) 111363.

[36] L. Baringthon, T.H. Dang, H. Jaffrès, N. Reyren, J.-M. George, M. Morassi, G. Patriarche, A. Lemaitre, F. Bertran, P. Le Fèvre, Topological surface states in ultrathin $Bi_{1-x}Sb_x$ layers, Phys. Rev. Mater. 6 (2022) 074204.

[37] A. Arnoult, J. Colin, Magnification inferred curvature for real-time curvature monitoring, Sc. Rep. 11 (2021) 9393.

[38] C.J. Kirkham, V. Bràzdová, D.R. Bowler, Bi on the Si(001) surface, Phys. Rev. B 86 (2012) 035328.